NRC Publications Archive
Archives des publications du CNRC

Melt compounding of different grades of polystyrene with organoclay : Part 1 : Compounding and characterization

Tanoue, Shuichi; Utracki, Leszek A.; Garcia-Rejon, Andrés; Tatibouët, Jacques; Cole, Kenneth C.; Kamal, Musa R.

NRC Publications Record / Notice d'Archives des publications de CNRC:

https://nrc-publications.canada.ca/eng/view/object/?id=98ada9ac-0044-4af1-b212-868bf563bbe6
https://publications-cnrc.canada.ca/fra/voir/objet/?id=98ada9ac-0044-4af1-b212-868bf563bbe6

National Research Council Canada   Conseil national de recherches Canada

Canada

Melt Compounding of Different Grades of Polystyrene With Organoclay. Part 1: Compounding and Characterization

SHUICHI TANOUE[1]*, LESZEK A. UTRACKI[2], ANDRÉS GARCIA-REJON[2†],
JACQUES TATIBOUËT[2], KENNETH C. COLE[2], *and* MUSA R. KAMAL[3]

[1]*Department of Materials Science and Engineering*
University of Fukui, 3-9-1 Bunkyo, Fukui 910-8507, Japan

[2]*Industrial Materials Institute, National Research Council Canada*
75 de Mortagne, Boucherville, QC J4B 6Y4, Canada

[3]*Department of Chemical Engineering, McGill University*
3610 University Street, Montreal, QC H3A 2B2, Canada

Nanocomposites of polystyrene (PS) with up to 20 wt% organoclay were prepared by melt compounding in a co-rotating, intermeshing twin-screw extruder. Three grades of PS with different molecular weights were used. In this paper we discuss preparation and characterization of the mixtures. Residence time and its distribution were measured by ultrasonics (US). They were found to be independent of the PS grade, but the US attenuation and sound velocity varied with the organoclay loading. According to the XRD diffraction data, the organoclay was dispersed into two types of platelet stacks evidenced by the diffraction peaks at about $2\theta = 2.1$ and $5.5°$, i.e., with the interlayer spacings of $d_{001} = 4.20$ and 1.6 nm, respectively. Since neat organoclay has $d_{001} = 1.93$ nm, the first peak indicates intercalation by PS and the other a collapse of the interlamellar gallery during compounding. The XRD spectra depended on the organoclay content, but not on PS grade. According to TEM analysis, the degree of intercalation of organoclay in the polymer matrix is highest for the low-molecular-weight polystyrene. TEM results also confirm the collapse of interlamellar spacing in parts of the samples. FT-IR spectroscopy showed that there was some thermal degradation of the onium compound present in the nanoclay. Polym. Eng. Sci. 44:1046–1060, 2004. © 2004 Society of Plastics Engineers.

INTRODUCTION

Polymer/clay nanocomposites (PNC) consist of inorganic layered clay dispersed in a polymeric matrix. To maximize the effect of nanofiller on performance, it is important that the clay is exfoliated. This may be accomplished in two steps: (i) intercalation of clay by an organic modifier, and (ii) exfoliation of the intercalated clay either during polymerization (reactive exfoliation) or during mechanical compounding in a melt mixer (mechanical exfoliation).

In systems containing nanometer-size particles, the total interfacial area is large (the specific surface area of montmorillonite is about 750 m^2/g). Since the clay platelets also have large aspect ratio (e.g., $p =$ diameter/thickness $\cong 100$ to 500), the interactions between them at loadings $w > 1.2$ wt% may be too large for free rotation and random distribution. Thus, at higher clay concentration, local ordering of platelets is expected and the motion of polymer molecules between them is restricted. This is the basic mechanism that leads to the excellent performance of PNC; the mechanical and thermal properties of a polymer can be significantly improved by dispersing in it a small amount of nanometer-size clay platelets. In addition, other properties, for example gas barrier, flame retardancy, moldability, surface finish, etc., are also improved (1, 2).

Kojima *et al.* (3) demonstrated these effects for nanocomposites of polyamide-6 (PA-6) with clay. Because the amount of clay is low (usually 1 to 5 wt%), the density of PNC is increased by ca. 1%. This is one of the principal differences between PNC and traditional composites containing, e.g., glass fiber or reinforcing mineral

filler. In addition, the nanocomposites can be prepared at relatively low cost and processed using standard manufacturing equipment.

The mechanical exfoliation of PNC is usually performed in two steps: (i) clay intercalation, which by inserting organic molecules between platelets changes clay from hydrophilic to organophilic, and (ii) exfoliation during melt compounding with a polymeric matrix. The key to the success is miscibility of the intercalant with the polymeric matrix, and its thermal stability under the processing conditions.

Exfoliation of clay platelets by polar polymers with groups capable of strong interactions with the clay platelets (e.g., polyamide or epoxy resin) has been successful. In particular, the PA-6/clay PNC have been the most studied systems since the late 1980s, when these nanocomposites (containing 2 to 5 wt% of organoclay) were introduced by the Toyota Central Research & Development Laboratories (4−6). Today, several chemical or plastic companies manufacture these nanocomposites (viz. Bayer, Clariant, Honeywell, Nanocor, RTP Co., Showa Denko, Ube Intl., Unitika, etc.). By contrast, it is much more difficult to exfoliate clay in a nonpolar polymer such as polystyrene (PS) or polypropylene (PP). In these cases, it might be necessary to use a compatibilizer to enhance miscibility between non-polar polymer and the clay.

PS is an important commodity polymer, along with others such as polyethylenes, polypropylenes, acrylics, and vinyls. Polymerization in the presence of organoclay has been carried out in bulk (using free radical and coordination methods), as well as in emulsion, suspension, and solution. The reaction most often leads to clay exfoliation. However, there are several disadvantages: 1) the reaction is slow (it may take more than 24 h), 2) exfoliation is not thermodynamically stable and the platelets re-aggregate during subsequent processing or forming steps, and 3) the process is available only to the resin manufacturer who is able to dedicate a production line for this purpose (clay is catalytically active). To bypass problems 1 and 2, PS-based PNC were prepared starting with organoclay pre-intercalated with a vinyl-terminated reactive compound, viz. vinyl benzyl *di*-methyl dodecyl ammonium chloride (7, 8), vinyl *tri*-ethoxy silane (used with cetyl pyridium chloride) (7), or vinyl benzyl *di*-methyl ethanol ammonium chloride (9). A high degree of exfoliation was obtained, the dispersion of the end tethered clay platelets was stable, but the reaction still required 15 h.

Mechanical exfoliation has several advantages: it is rapid (< 10 min), since it is controlled by the thermodynamic interactions there is no danger of re-aggregation during the forming stage, and the process is available to anyone having a suitable mixer, e.g., a twin-screw extruder (TSE). The main disadvantage is the need for thermally stable (at the processing conditions) organoclay, which is readily miscible with the polymeric matrix.

During the last few years many research groups studied the melt intercalation/exfoliation of PS/clay nanocomposites. Hasegawa *et al.* (10) produced exfoliated

PS-clay nanocomposites by compounding PS with organoclay and a compatibilizer in a TSE. The organoclay was montmorillonite (MMT) pre-intercalated with trimethyl octadecyl ammonium chloride (3MODA), while the compatibilizer was poly(styrene-*co*-methyl vinyl oxazoline). Hoffmann *et al.* (11) used synthetic fluoromica pre-intercalated with either 2-phenylethylamine (PEA) or with amine-terminated polystyrene (AT-PS; M_n = 5.8 kg/mol). The PNC was prepared by compounding 5 wt% of organoclay with PS at 200°C in a micro-compounder. According to XRD, the PNC with PEA did not intercalate, viz. d_{001} = 1.4 nm, but the one prepared with AT-PS was exfoliated (d_{001} > 4 nm); the observation was confirmed by TEM. The latter system was end tethered, similar to the "classical" PA-6/clay nanocomposites from Toyota or Ube.

Park *et al.* (12) manufactured PNC with syndiotactic PS as the matrix and Cloisite® 15A (MMT intercalated with *di*-methyl *di*-hydrogenated tallow alkyl ammonium chloride, 2M2HTA). Owing to thermal instability of the organoclay at the sPS processing temperatures a two-step process was used. First, the organoclay was compounded in an internal roller mixer at $T \cong$ 200°C with a compatibilizer, e.g., PS, SMA (random copolymer of styrene and maleic anhydride), or SEBS-MAH (styrene-ethylene-butylene-styrene block copolymer grafted with maleic anhydride). Second, a matrix polymer (sPS, SMA or SEBS-MA) was added at $T \cong$ 280°C and the material was homogenized. XRD, TEM and mechanical testing were used to characterize the products. The nanocomposites with SEBS-MA were exfoliated.

Yoon *et al.* (13) reported on the effects of polar comonomers and shear on the performance of PNC with PS matrix. PS and three commercial styrenic copolymers composed of styrene (ST), acrylonitrile (AN) and methyl-vinyl oxazoline (OZ) were used. The organoclay used was Cloisite® 10A (MMT intercalated with *di*-methyl benzyl hydrogenated tallow ammonium chloride, 2MBHTA). PNC with 5 wt% of Cloisite® 10A were prepared using either static annealing or compounding in an internal mixer at T = 210°C. Owing to thermal instability of the organoclay, the interlayer spacing initially expanded and then started to collapse from d_{001} = 3.5 to 1.9 nm. The effect was moderated by the presence of AN or OZ comonomer.

Direct mixing of PS with 1−10 wt% of Cloisite® 10A in an internal mixer was carried out at T = 180°C−200°C by Uribe *et al.* (14). The resulting interlayer spacing, $d_{001} \cong$ 3.6 nm, was virtually independent of the mixing conditions. The tensile measurements indicated that the presence of organoclay enhanced the modulus by ca. 70%, but reduced the tensile strength.

Several companies manufacture organoclay on the industrial scale. These commercial organoclays have been used by various researchers for the preparation of PS-clay nanocomposites by melt compounding in the extruder or internal mixer (14−17). Although intercalation of polymer matrix between clay platelets was realized in these studies, exfoliation was not achieved. Fornes *et al.* (15) studied the effect of the PA-6 matrix

molecular weight on the properties of nanocomposites, but similar studies on the melt compounding of non-polar polymers (e.g., PS or PP) have not been published.

The aim of this work was to explore a wide range of processing conditions for the preparation of PS/clay nanocomposites using a TSE. Commercial PS grades with different molecular weights (MW) were employed. The study used various compounding conditions and characterization techniques to determine the effects of MW and processing variables on PS/clay mixtures. Moreover, the study involved the evaluation of an in-line ultrasound monitoring system to follow some process variables during the preparation of PNC. This technique was found useful in monitoring the melt compounding of polymer blends or filled systems (16, 17). Ultrasonics have been used to determine the residence time and its distribution in extruders (18, 19), to monitor stability of polymer coextrusion (20) and extrusion foaming (21). It was hoped, in the present study, to explore the utility of in-line ultrasound monitoring in the preparation of polystyrene/clay nanocomposites.
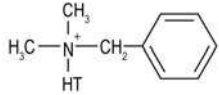
EXPERIMENTAL

Materials

Three grades of commercial PS used in this study were supplied by Nova Chemicals (Pittsburgh, PA). Their weight average molecular weight (M_w) and melt flow rate (MFR) are listed in *Table 1*. In the following text the three resins are coded as LMW, MMW and HMW, for low, medium and high M_w grade, respectively. The selected organoclay is Cloisite® 10A, purchased from Southern Clay Products (Gonzales, TX). This organoclay is a MMT (cation exchange capacity CEC = 0.926 meq/g, d_{001} = 1.17 nm) intercalated with 1.25 meq/g of *di*-methyl benzyl hydrogenated tallow ammonium chloride (2MBHTA), which increased the interlayer spacing to d_{001} = 1.92 nm. Other properties are listed in *Table 1*.

Melt Compounding of Polystyrene With Organoclay

Three series of PS based PNC were prepared in a Leistritz co-rotating twin-screw extruder TSE-34 (*L/D* = 40). Compounding was carried out at a uniform barrel temperature of 200°C, a screw speed of 200 rpm, and a feed rate of 5 kg/h. Organoclay was added to molten polymer using a side feeder. Screw configurations and locations of the hopper and the side feeder are shown in *Fig. 1*. *Table 2* shows the extrusion conditions used for the preparation of the PS/organoclay mixtures.

The organoclay content in these PNC was determined by TGA. Comparing these values with those estimated

Table 1. Material Characteristics.

Material (Code)	Supplier	Specification
Polystyrene 1220 (HMW PS)	NOVA Chemicals	M_w = 310 kg/mol MFR[1] = 1.9 g/10 min
Polystyrene 1301 (MMW PS)	NOVA Chemicals	M_w = 270 kg/mol MFR[1] = 3.5 g/10 min
Polystyrene 1510 (LMW PS)	NOVA Chemicals	M_w = 230 kg/mol MFR[1] = 6.5 g/10 min
Organoclay (Cloisite® 10A)	Southern Clay Products, Gonzales, TX	Na-MMT[2] intercalated with 2MBHTA[3]: Organic loading = 1.25 meq/g Organic content = 39 wt% Interlayer spacing: d_{001} = 1.92 nm

Notes: [1]Measured by ASTM D1238, Procedure B; 200/5.0;
[2]CEC = 0.926 meq/g; interlayer spacing: d_{001} = 1.17 nm;
[3]2MBHTA = di-methyl, benzyl hydrogenated tallow ammonium chloride (tallow contains: ~65% C_{18}; ~30% C_{16}; ~5% C_{14}).

from the feeding rates of PS and organoclay resulted in the determination of the feeding errors calculated from the following equation:

$$Error\,(\%) = 100 \times \frac{(moc) - (coc)}{(coc)} \qquad (1)$$

where *moc* represents measured organoclay content and *coc* represents calculated organoclay content.

The error decreases with increase of organoclay content (see *Table 2*). At the low organoclay content (about 1 wt%) the error is 40%~50%, whereas at high (about 10 wt%) it is ca. 20%. The error mainly originates from inaccuracy of the side feeder at the low feed rates; the lowest, stable feed rate is 0.2 kg/h. Furthermore, the feeder was miscalibrated as the error is non-random, biased by about 25%.

A schematic of the equipment used for the preparation of nanocomposite is shown in *Fig. 2*. The special slit die attached to the extruder is shown in *Fig. 3*. The die houses two US probes, three pressure transducers and two thermocouples. The setup has been used for different extrusion monitoring experiments. However, its main use during the experiments discussed in this paper was for the in-line measurement of the residence time and its distribution during extrusion compounding of the PS/organoclay PNC. The detailed information on the method is published elsewhere (18). The applied US frequency was 5 MHz.

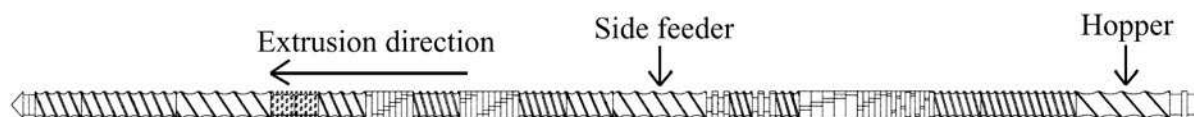Extrusion direction ←   Side feeder ↓   Hopper ↓

Fig. 1. Screw configurations and the location of the side feeder for adding organoclay into polymer matrix and the hopper for feeding the polymer pellets.

Table 2. Extrusion Conditions.

PS	Side Feeder Feed Rate (kg/h)	Organoclay Content[1] (wt%)	Organoclay Content[2] (wt%)	Organoclay Feed Rate Error (%)
HMW PS	0	0	0	0
	0.05	1.0	1.3	30
	0.1	2.0	2.5	25
	0.25	4.8	5.6	17
	0.5	9.1	11.1	22
MMW PS	0	0	0	0
	0.05	1.0	1.4	40
	0.1	2.0	2.8	40
	0.25	4.8	5.7	19
	0.5	9.1	10.6	16
LMW PS	0	0	0	0
	0.05	1.0	1.5	50
	0.1	2.0	2.1	5
	0.25	4.8	6.0	25
	0.5	9.1	10.6	16

Notes: Compounding conditions: barrel temperature 200°C, screw rotation speed 200 rpm, PS feed rate 5 kg/h;
[1]Calculated from the nominal hopper feed rate and that of side feeder;
[2]Inorganic content determined by TGA, then the organoclay concentration calculated assuming organic content in Cloisite® 10A as 39 wt%.
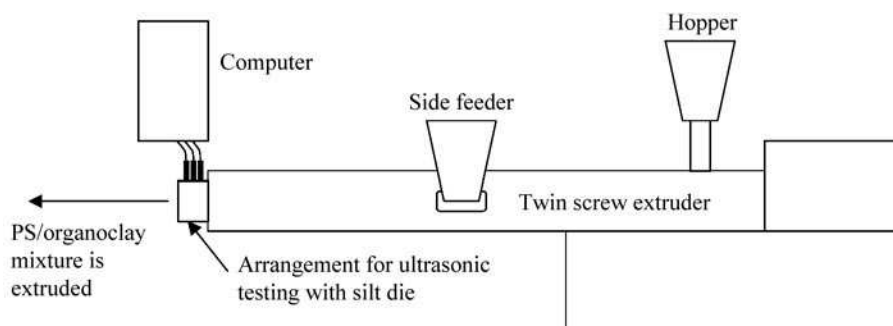

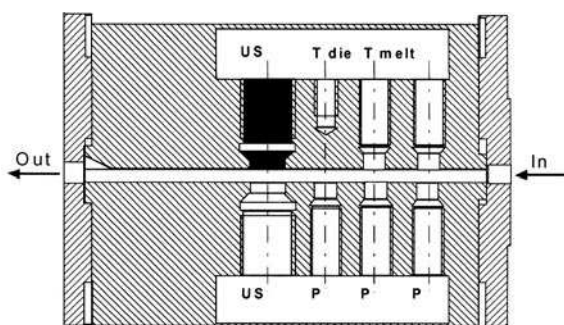Fig. 2. Illustration of equipment used for the preparation of nanocomposite.

Fig. 3. Typical arrangement of a slit die, showing location of ultrasonic probes, US, thermocouples (T_{die}, T_{melt}) and pressure probes (P) (16).

As described by Piché *et al.* (22), the US probes make it possible to determine the ultrasound propagation characteristics (attenuation and velocity) across the polymer flowing through the slit die. For the tests, the die was installed at the exit of a TSE (see *Fig. 2*). To determine the residence time and its distribution, a small amount of $CaCO_3$ was used as the tracer. Furthermore,

in-line ultrasonic monitoring was carried out during the preparation of the PNC listed in *Table 2*.

PVT Measurements

The *PVT* behavior was measured in a Gnomix apparatus (Gnomix Inc., Boulder, CO), within a range of temperatures ($T = 300-520$ K) and pressures ($P = 0.1$ to 190 MPa). The molten state was observed within the temperature range from about 360 to 520 K. Considering hygroscopicity of the clay, the material was dried for 48 hrs at 80°C prior to testing and the subsequent handling of the resin was carried out in a glove compartment under positive pressure of dry N_2. Since the instrument measures only the incremental changes of the specific volume as a function of *P* and *T*, first an absolute value of the specific volume at ambient condition was measured with accuracy of $\Delta V \leq \pm 0.001$ mL/g.

To ensure a high degree of reliability, for each resin between two and five isothermal runs were carried out. During these runs the temperature was set and $V = V(P)$ was determined, then *T* was changed and the process repeated. Thus, this procedure minimized exposure of

the tested compositions to high temperature. A high degree of reproducibility was obtained.

Characterization of Nanocomposites

The PS/organoclay extrudates were characterized by X-ray diffraction (XRD), transmission electron microscopy (TEM), and Fourier transform infrared spectroscopy (FT-IR). The XRD measurements were carried out using a Rigaku Rotaflex X-ray diffractometer with Cu-rotation anode and Theta/2Theta scan. XRD scans were obtained using an incident X-ray wavelength $\lambda = 0.15406$ nm at a scan rate of $1.5°$/min. For these tests the specimens were prepared by compression molding at temperature, $T = 200°C$, and compressive force, $F = 5$ tons.

The microstructure of PS/organoclay mixtures was examined by TEM. The samples were all microtomed at room temperature with a diamond knife using a Leica Ultracut FC microtome. The nominal thickness of the sections was 70 nm. The sections were transferred from water to 200-mesh Cu grids. Low-magnification bright-field pictures (5000×) were taken with a JEOL 2000FX at an acceleration voltage of 80 kV. The micrographs were digitally imaged with a charge coupled device (CCD) camera (Gatan Bioscan). High-magnification pictures (100,000×) were taken with a JEOL JEM 2011 at an acceleration voltage of 200 kV. The micrographs were recorded on photographic negatives—Kodak electron microscope film Estar Thick base 4489—and enlarged 5× for the prints. To ensure a representative analysis of the materials, several pictures were taken over 3 to 4 sections per grid.

For the FT-IR measurements, thin films were prepared by rapid hot pressing at 170°C. Transmission spectra were measured on a Thermo Nicolet Magna 860 spectrometer with DTGS detector, at a resolution of 4 cm^{-1} and with an accumulation of 128 scans.

RESULTS

Residence Time and Its Distribution

Figure 4 shows the residence time distribution curves for the three grades of PS flowing from the hopper to the exit of the extruder as well as from the side-feeder to the die. The numerical values are listed in *Table 3*. As shown in *Fig. 4*, the residence time distribution curves for the three polymers are almost the same. The peak position moves slightly to shorter time as the M_w of PS increases. Similar results were obtained for the
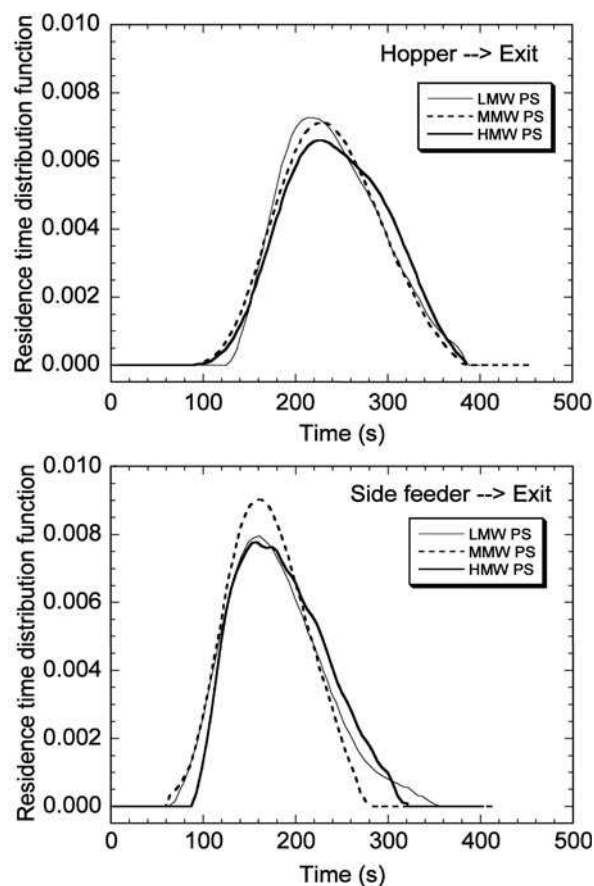

Fig. 4. Comparison of residence time distributions for three PS resins in a TSE at feeding rate of 5 kg/h, screw rotation speed of 200 rpm and barrel temperature of 200°C.

residence time distribution from the side-feeder to the exit. Again, the data for the three PS grades virtually superimposed one on top of another.

Ultrasonic Monitoring

For viscoelastic polymers, the US velocity and the attenuation are related to the storage and loss moduli, respectively (21):

$$v_{visc} = \sqrt{\frac{M'}{\rho}} \qquad (2)$$

$$a_{visc} = \frac{M''\omega}{2\rho v_{visc}^3} = \frac{\omega}{2v_{visc}}\tan\delta \qquad (3)$$

Table 3. Mean Residence Time $\bar{t}$ and Its Normalized Variance σ^2 for Flow From the Hopper to the Die and From the Side-Feeder to the Die.

PS	Flow From Hopper to Die		Flow From Side-Feeder to Die	
	$\bar{t}$ (s)	σ^2	$\bar{t}$ (s)	σ^2
LMW PS	236	0.0448	179	0.0828
MMW PS	237	0.0494	169	0.0605
HMW PS	234	0.0475	185	0.0662

where v_{visc} and a_{visc} are the US velocity and attenuation of viscoelastic polymer, M' and M'' are its bulk storage and loss moduli, ρ is polymer density and ω is the angular frequency as $\omega = 2\pi f$, where f is the frequency in Hz. This means that ultrasound probes the viscoelastic properties of the materials and that sound velocity and attenuation depend on viscosity and structural state of the polymer melt.

Figure 5 shows the US velocity and attenuation measured in-line at the exit of the extruder as a function of organoclay content for PS based mixtures. All the velocity values are corrected for pressure dependence and normalized at 6.89 MPa. The sound velocity decreases with increase of organoclay loading and the attenuation increases with organoclay content. This behavior has been observed for other filled systems (23), and it can be attributed to viscous dissipation around the filler particle interacting with the ultrasonic wave. The decrease of velocity with M_w of PS (by $\pm 0.5\%$) might be
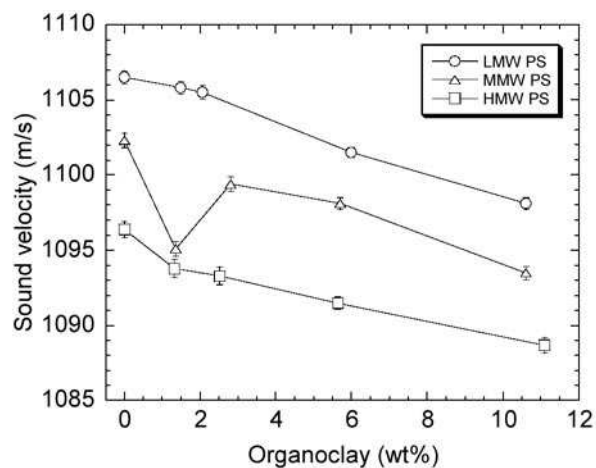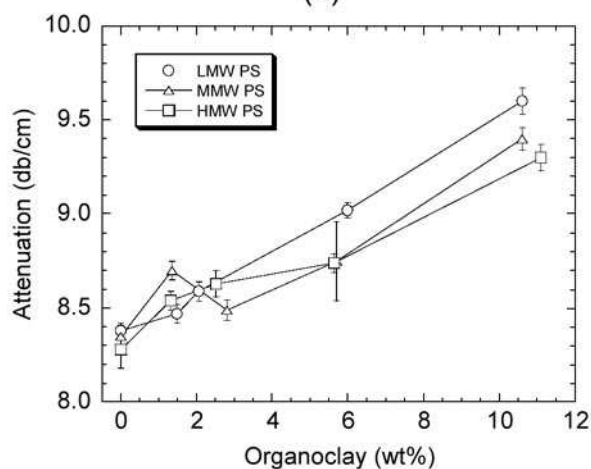
Fig. 5. In-line ultrasonic test results at the exit from a TSE as a function of organoclay content for the three PS based PNC: (a) sound velocity; (b) attenuation.

attributed to difference in the actual temperature of these melts, possibly the more viscous resin having higher temperature by the increased shear heating during flow through the slit die.

X-ray Diffraction (XRD)

From the nominal interlayer spacing d_{001} of organoclay used in this study (1.92 nm), the main diffraction peak position of the organoclay can be calculated from Bragg's formula as $2\theta = 4.6°$:

$$d_{00n} = n\lambda/(2 \sin \theta) \qquad (4)$$

where, n is an integer, θ is the angle of incidence (or reflection) of X-ray beam, and λ is the X-ray wavelength. In these experiments, $\lambda = 0.15405$ nm (Cu-Kα) was used. Similarly, *Eq 4* gives the peak position for the non-intercalated clay where $d_{001} = 1.17$ nm as $2\theta = 7.5°$.

Figure 6 shows XRD scans for the PNC based on the three grades of PS. The scans show two peaks particularly strong at high organoclay content (about 10 wt% in *Fig. 6d*). One peak is located at $2\theta < 4.6°$ and the other is located at $2\theta > 4.6°$. The former is named the 1st peak and the latter is the 2nd peak. The intensity of the 2nd peak is larger than that of the 1st for all organoclay contents and PS grades. At low organoclay loading the 1st peak is invisible, suggesting that some organoclay may be exfoliated. Evidently, the magnitude of the peak increases with the organoclay content, but the increase is not directly proportional to loading.

Transmission Electron Microscopy (TEM)

Typical micrographs obtained by TEM are shown in *Fig. 7* for samples of each of the three materials. The figure shows both low-resolution micrographs to indicate the quality of distributive mixing and high-resolution micrographs to evaluate the extent of intercalation or exfoliation. In the former the quality of distributive mixing is reasonably good. However, it is obvious from these micrographs that some large agglomerates persist. The d_{001} spacing as estimated from the high-resolution micrographs is shown in *Table 4*. It suggests that the spacing increases as the molecular weight of the polymer decreases.

Fourier Transform Infrared Spectroscopy (FT-IR)

FT-IR can give useful information on chemical changes occurring in the system. However, the detection of such changes can be challenging because often the new species produced are present in small amounts and they are chemically similar to the initial material, so their absorption peaks are masked. To facilitate the detection of small changes, difference spectra were calculated for the extruded samples by subtracting out the spectrum of the corresponding neat PS. The resulting difference spectra were then scaled to correspond to a common film thickness. Because of strong absorption by PS or clay in certain regions of the spectrum, the useful information is limited to the windows shown in *Fig. 8*.
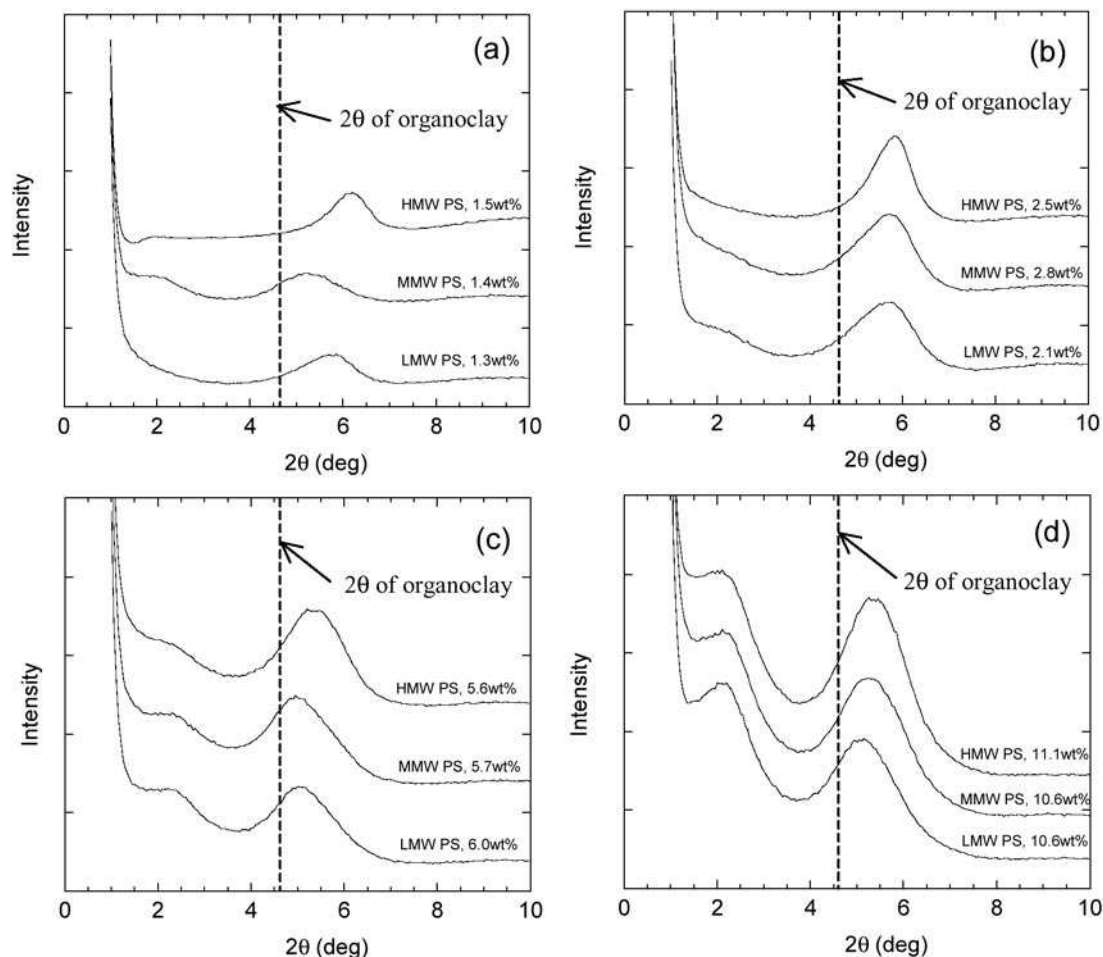
Fig. 6. XRD diffraction data for PS based organoclay mixtures at various organoclay contents: (a) about 1 wt%, (b) about 2 wt%, (c) about 5 wt% and (d) about 10 wt%.

Pressure-Volume-Temperature (PVT)

For each resin, two to five isothermal runs were carried out. During these runs the temperature, T, was set at a specified level and $V = V(P)$ was determined; then T was increased and the process repeated up to the set maximum T-value. To illustrate the reproducibility, *Fig. 9* shows the PVT surface, $V = V(P, T)$, for PS1301 (MMW) with 2.8 wt% of Cloisite® 10A. Note the excellent superposition of data for two runs in the whole range of independent variables: $T = 360$ to 520 K and $P = 1$ to 1900 bar. Similar agreement was observed for other compositions.

The PVT behavior is best described using the Simha-Somcynsky (S-S) equations of state (eos) (24, 25). The model assumes amorphous assembly of chain molecules on a lattice with sites occupied either by segments or vacancies (holes). The directly incorporated hole fraction, h, is a measure of the free volume. The configurational thermodynamic properties are then characterized by three quantities, i.e., the maximum attraction energy between a pair of chain segments, ε^*, the corresponding segmental repulsion volume, v^*, and the number $3c$ of volume dependent, external degrees

of freedom. In terms of these quantities and the number s of segments per chain, the three characteristic pressure, temperature and volume parameters can be defined, viz.

$$P^* = zq\,\varepsilon^*/(sv^*); \quad T^* = zq\,\varepsilon^*/Rc; \quad V^* = v^*/M_s \quad (5)$$

with M_s the molar segmental mass, $zq = s(z - 2) + 2$, the number of interchain contacts in a lattice of coordination number $z = 12$, and R the gas constant. The variables of state, P, T, V, are then scaled by P^*, T^*, V^*, to define a universal, reduced $\widetilde{P} - \widetilde{T} - \widetilde{V}$ surface, common to all liquids. The S-S theory yields a reduced Helmholtz free energy function, $\widetilde{F}$, as:

$$\widetilde{F} = \widetilde{F}\,[\,\widetilde{V},\,\widetilde{T},\,h(\widetilde{V},\,\widetilde{T}\,)\,] \quad (6)$$

From *Eq 6* the hole fraction, h, is obtained by minimizing the free energy at a specified volume and temperature:

$$(\partial\widetilde{F}/\partial h)_{\widetilde{V},\,\widetilde{T}} = 0 \quad \Rightarrow$$

$$3c\,[(\eta - 1/3)/1 - \eta) - yQ^2\,(3.033Q^2 - 2.409)/6\widetilde{T}\,]$$

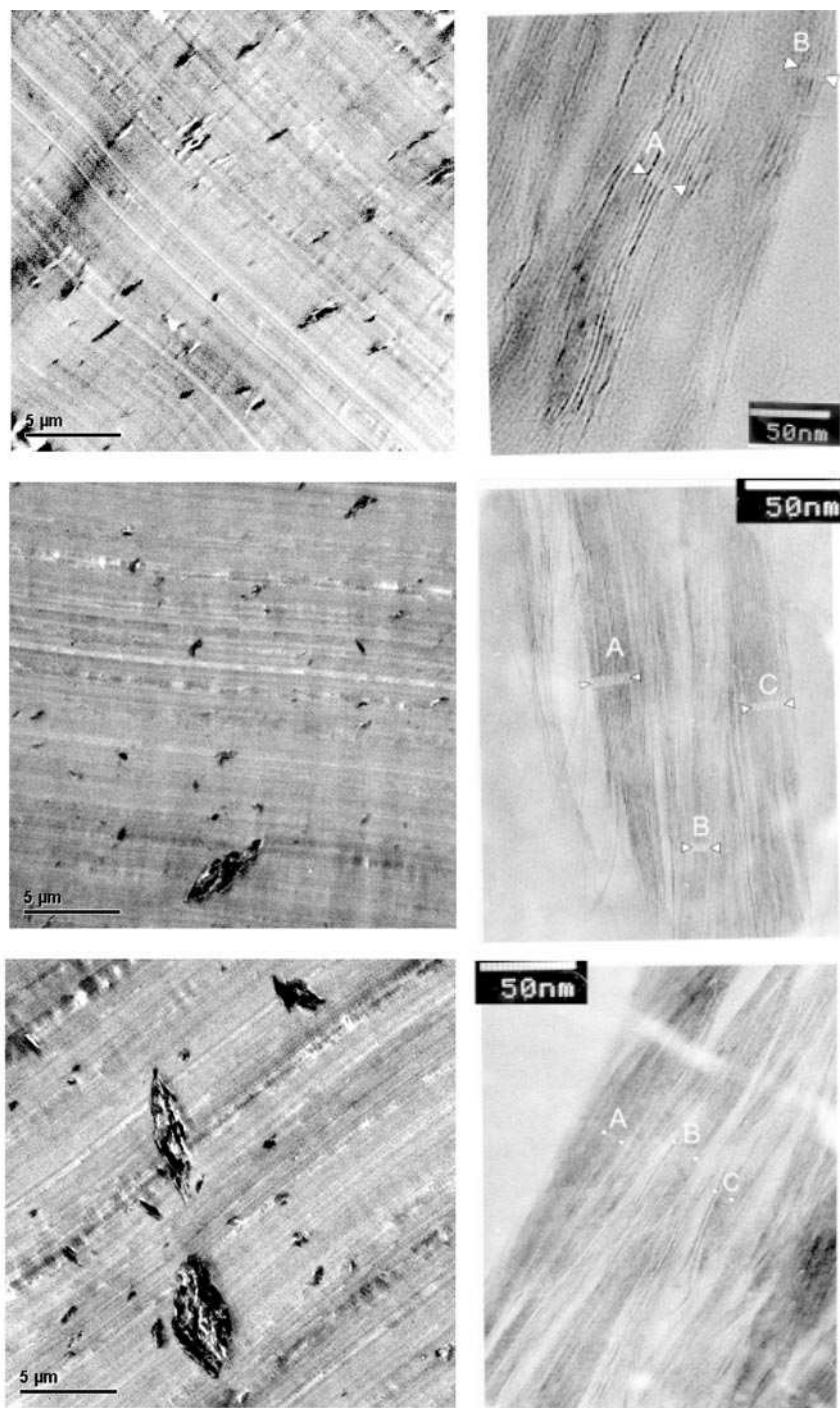$$+ (1 - s) - (s/y)\,\ell n\,[(1 - y)] = 0 \quad (7)$$

Fig. 7. Typical TEM micrographs for PS with 2 wt% organoclay. The three rows are for (from top) HMW, MMW and LMW PS, respectively. The left column is for low magnification (scale bar 5 μm), while the right column is for high magnification (scale bar 50 nm). On the latter micrographs the letters A, B, C indicate the place where the interlayer spacing was calculated.

and the reduced pressure is obtained as:

$$\widetilde{P} = -(\partial \widetilde{F}/\partial \widetilde{V})_{\widetilde{T}} \quad \Rightarrow$$

$$\widetilde{P}\widetilde{V}/\widetilde{T} = (1-\eta)^{-1} + 2y Q^2 (1.011 Q^2 - 1.2045)/\widetilde{T} \quad (8)$$

with $y = 1 - h$; $Q = 1/(y\widetilde{V})$; $\eta = 2^{-1/6} y Q^{1/3}$, and for macromolecules $(s \gg 1)$ $3c/s \to 1$.

The determination of the reducing parameters from experimental data proceeds by simultaneous fit of *Eqs 7* and *8*. The computations have been performed using MicroMath *Scientist*™ commercial software, which minimizes the differences between the experimental data and the theory by the non-linear least-squares algorithm. Data from all runs of a given composition were

Table 4. Calculation of the Interlayer Spacing in PS With About 2 wt% Organoclay From the High-Resolution TEM Images (Shown in *Fig. 7*).

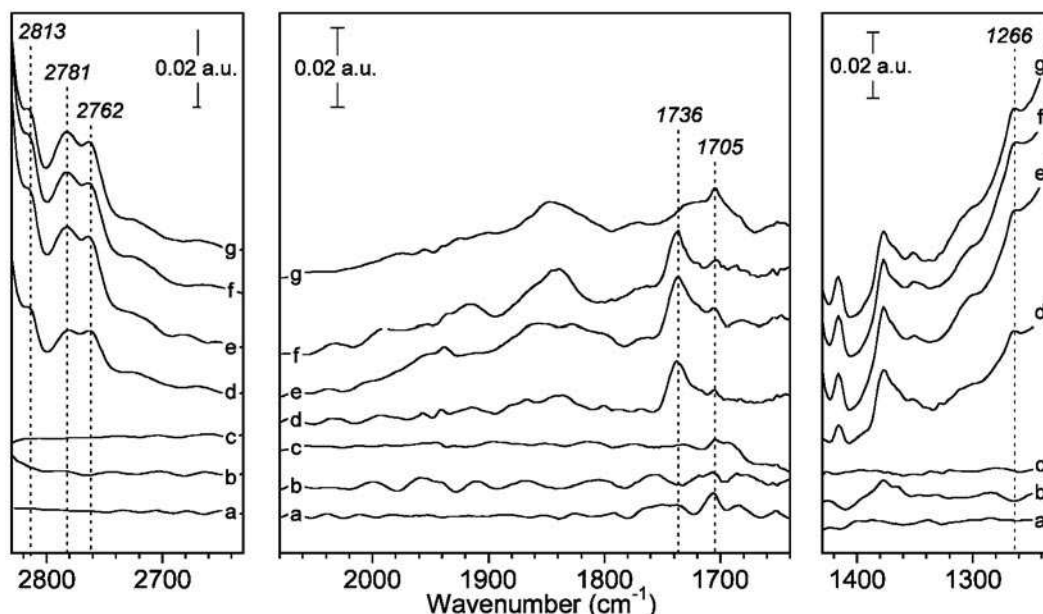| Sample	Measurement	Length (nm)	Number of Platelets	d_{001} (nm)
HMW PS Organoclay 2.5 wt%	A	5.21	5	1.30
	B	8.37	8	1.20
	C	4.03	4	1.34
	Average interlayer spacing:			1.28
MMW PS Organoclay 2.8 wt%	A	18.59	14	1.43
	B	8.03	7	1.34
	C	16.29	13	1.36
	Average interlayer spacing:			1.35
LMW PS Organoclay 2.1 wt%	A	14.45	5	3.61
	B	14.72	6	2.94
	Average interlayer spacing:			3.28

Fig. 8. Difference spectra obtained for various extruded samples by subtracting the spectrum of neat PS: (a) LMW, 0 wt% clay; (b) MMW, 0 wt% clay; (c) HMW, 0 wt% clay; (d) MMW, 5.7 wt% clay; (e) LMW, 10.6 wt% clay; (f) MMW, 10.6 wt% clay; (g) HMW, 11.1 wt% clay.
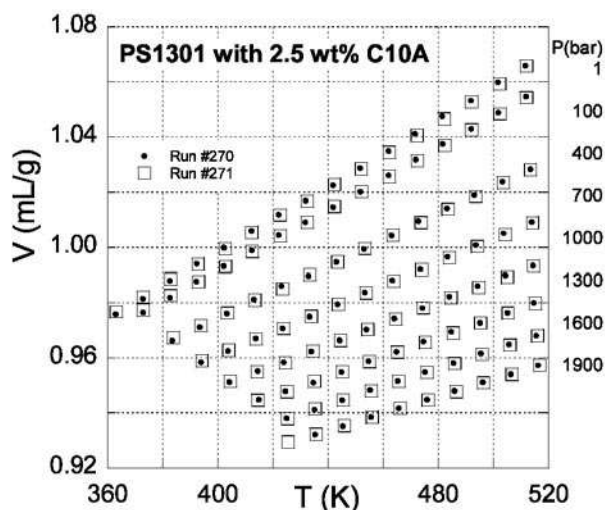

Fig. 9. Specific volume of PS1301 with 2.8 wt% of Cloisite® 10A as a function of temperature and pressure.

used to determine the characteristic reducing parameters, P^*, V^*, and T^*. The resulting parameters are listed in *Table 5*.

DISCUSSION

Melt Intercalation

The mean residence time $\bar{t}$ and its normalized variance σ^2 were computed from the residence time distribution curves using the following equations:

$$\bar{t} = \int_0^\infty t\, E(t)\, dt \qquad (9)$$

$$\sigma^2 = \frac{\sigma_t^2}{\bar{t}^2} = \frac{\int_0^\infty (t - \bar{t})^2\, E(t)\, dt}{\bar{t}^2} \qquad (10)$$

**Table 5. Statistics of Fitting the Simha-Somcynsky eos to Experimental Data
and the Computed Parameters for PS, and PNC Containing 1.4 to 17.1 wt% Cloisite® 10A.**

Organoclay content (wt%):	0	1.4	2.8	5.7	10.6	17.1
σ	0.0011119	0.0014205	0.0009326	0.0014970	0.0023897	0.0025876
r^2	0.9999987	0.9999980	0.9999991	0.9999977	0.9999939	0.9999924
Correlation	0.9994420	0.9990610	0.9995868	0.9989405	0.9971886	0.9967893
P^* (bar)	7435 ± 26	7492 ± 52	7475 ± 32	7556 ± 56	7471 ± 84	7510 ± 89
T^* (K)	11723 ± 22	11938 ± 46	12010 ± 29	11975 ± 48	11834 ± 74	11711 ± 73
$10^4 \times V^*$ (mL/g)	9525.9 ± 4.7	9583.7 ± 9.6	9567.8 ± 5.9	9458.8 ± 9.8	9259.6 ± 15.1	9011.2 ± 14.6
M_o (g/mol)	45.869	46.079	46.537	46.433	47.407	47.770
$<\varepsilon_{ij}>$	32.488	33.084	33.284	33.187	32.796	32.455
$<v_{ij}>$	43.694	44.161	44.526	43.920	43.897	43.046

where $E(t)$ is the residence time distribution function. The values of $\bar{t}$ and σ^2 are nearly the same for all three grades of PS. The computational results are listed in *Table 3*.

The MFR of the three PS resins varied from 1.9 to 6.5 g/10 min. The measurements were also performed with PNC, a PS mixture containing 2.8 wt% organoclay. No significant difference was found between these data and those of neat PS. Thus, the residence time in the extruder is about the same for different grades of PS as well as organoclay concentration in the mixtures.

Fornes *et al.* (15) reported similar observations. The authors determined the residence time distribution for three PA-6 resins with MFR = 1.2, 4.5 and 23. The data for the middle and high molecular weight PA-6 (MFR = 4.5 and 1.2, respectively) were the same within the range of experimental error, but those for the low molecular weight (MFR = 23) showed longer residence time and broader distribution. Thus, for viscous resins or mixtures the residence time and its distribution seem to depend on screw configuration, and process variables (e.g., feed rate), but not on the molecular weight or nanofiller loading.

Dispersion of Clay Platelets

The ultrasonic (US) velocity (see *Fig. 5a*) measured by in-line US probes seemingly shows an opposite tendency to that expected on the basis of the increasing rigidity with filler loading, known for solid materials. However, while the decrease of US velocity at organoclay content from 0 to 10 wt% changes by about 0.8%, the increase of density is 4.6%; hence according to *Eq 2*, at 10 wt% organoclay loading M' did increase by about 3%.

Figure 5b shows that US attenuation increased with organoclay loading of 10 wt% by about 12%, which translates into increase of the loss modulus, M'', by about 9.7%. From the slope of this dependence one can estimate the hydrodynamic volume of dispersed particles in the three PS grades as equal to 3.3. This value is not far from the intrinsic viscosity of monodispersed hard sphere suspensions, $[\eta] = 2.5$ calculated by Einstein. Thus, US monitoring indicates that independently of the possible exfoliation effects, the compounding leaves

behind nearly spherical (the estimated aspect ratio (26), $p = 2.8$) stacks of nondispersed organoclay.

Figure 6 displays the XRD spectra for selected PNC with the three PS resins. From these results, the interlayer spacing, d_{001}, can be calculated using *Eq 4*. In *Fig. 10* the value of d_{001} calculated from the position of the two peaks is plotted as a function of organoclay
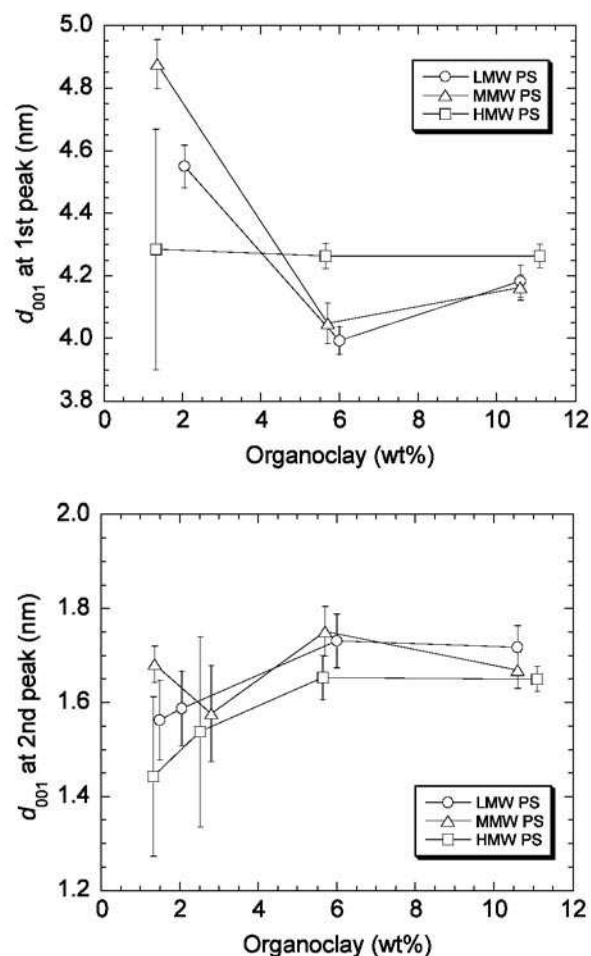

Fig. 10. Interlayer spacing, d_{001} (nm), of the 1st and 2nd peak as a function of organoclay content for the three PS based matrix resins.

content. It was quite difficult to estimate the interlayer spacing of the 1st peak at low organoclay loading in HMW PS. Considering the general tendency shown by the d_{001} vs. organoclay content, it seems reasonable to expect partial exfoliation for these compositions. The calculated d_{001} values are listed in *Tables 4* and *6*.

Within the experimental error of these measurements, the interlayer spacing is found to be independent of PS grade, but it changes with organoclay content. The interlayer spacing of the 1st peak decreases with an increase of organoclay content and it reaches a plateau at organoclay concentration exceeding 5 wt%. This is expected on the basis of geometric crowding argument confirmed by experimental data of, e.g., Okada and Usuki (6). By contrast, the interlayer spacing of the 2nd peak increases with organoclay content from the extrapolated value at zero-loading of $d_{001} = 1.3 - 1.4$ nm to 1.65 ± 0.05 nm. For HMW-based mixtures this spacing is the smallest.

The 1st peak indicates that during compounding the organoclay has been in part intercalated by PS macromolecules. Furthermore, the disappearance of this peak at the lowest organoclay loadings may indicate that some exfoliation did take place. However, the 2nd peak is dominant and, comparing its location to that of neat organoclay, it shows reduction of the interlamellar gallery height. There are two possible mechanisms for this to occur: 1) extraction of the intercalant from the interlamellar space, and 2) decomposition of the onium intercalant by the Hofmann elimination mechanism:
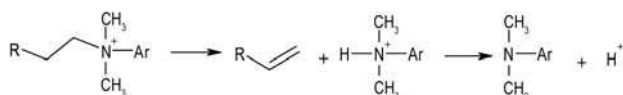
Comparing the CEC of MMT with the intercalant loading (see *Table 1*) it can be calculated that Cloisite® 10A has 35% excess of the 2MBHTA intercalant—its extraction would reduce the interlayer spacing to 1.66 nm; hence this mechanism does not explain the reduced spacing at low clay loading.

Several researchers reported that MMT intercalated with a long chain aliphatic quarternary ammonium cation is unstable at temperatures above 180°C or 200°C (13, 27–29). In particular, Zhu *et al.* (28) studied the thermal stability of PS prepared with MMT intercalated with either ammonium or phosphonium cation. The data indicated that the former compound decomposed at $T > 200°C$, resulting in reduction of the interlamellar gallery height—a broad XRD peak was observed with the interlayer spacing of $d_{001} = 1.58$ nm. Thus, when the processing temperature is high, thermal degradation of the organoclay intercalant causes reduction of the interlamellar gallery and the re-aggregation of clay platelets.

The FT-IR results in *Fig. 8* provide clear evidence of such thermal degradation. The extruded neat PS show only very weak features (including some interference fringes), whereas the extruded samples containing clay show a number of distinct peaks. Some of these peaks are also seen in the spectrum of Cloisite® 10A and arise

from the 2MBHTA of the onium compound. However, the peaks whose positions are labeled in *Fig. 8* correspond to species produced in the extrusion process. Those at 2813, 2781, and 2762 cm^{-1} correspond exactly to the strong C−H stretching vibrations of methyl and methylene groups in benzyl dimethyl amine (BDMA), one of the degradation products shown in the above equation (30). Although the onium salt also contains such groups, the presence of the lone pair of electrons on the nitrogen of the tertiary amine leads to a significant frequency shift and makes it possible to easily distinguish the two compounds (31). The peak at 1266 cm^{-1} can also be assigned to BDMA. In addition to the BDMA peaks, there is a strong carbonyl peak at 1736 cm^{-1} in most of the extruded samples containing clay. This probably corresponds to aldehyde or carboxylic acid groups formed by oxidation of the double bond in the long-chain olefin shown in the above equation. Finally, there is some evidence of a very weak peak at 1705 cm^{-1} that could be due to ketone carbonyl groups. Since it also appears to be present in the neat PS samples, it may be a product of PS degradation.

The peak position and the interlayer spacing related to it are only one part of the information provided by the XRD measurements. The other part is related to the intensity of the diffraction peak and its dependence on the concentration of scattering particles. Cullity and Stock (32) in their monograph on the X-ray diffraction derived the following relation for the intensity of the diffraction peak of α-substance mixed with another substance (β):

$$I_\alpha = K\phi_\alpha/[\phi_\alpha(\mu_\alpha - \mu_\beta) + \mu_\beta] \quad (11)$$

where ϕ_α is volume fraction of the diffracting substance α, and μ is the mass absorption coefficient. Depending on the relative magnitude of μ_α and μ_β within the full range of concentration, *Eq 11* predicts additivity, as well as positive or negative deviation from it. However, within the limited range of clay concentrations used in PNC, *Eq 11* predicts proportionality:

$$I_\alpha = K'w_\alpha I_{neat\,\alpha} \quad (12)$$

where K' is the proportionality factor not far from one, w_α is weight fraction of the α-substance in the mixture, and $I_{neat\,\alpha}$ is the intensity that would be observed for neat α-substance.

In accord with *Eq 12*, the spectra displayed in *Fig. 6* show that the intensity of XRD scattering increases with organoclay content. Within the range of interest, $2\theta_1 < 2\theta < 2\theta_2$, the XRD spectrum of neat PS is relatively featureless and flat (see *Fig. 11*). Taking it as a baseline for XRD of the PNC, the following "appearance factor" can be defined:

$$A_{clay}\Big|_w = A_{mix}\Big|_w - A_{PS} = \int_{2\theta_1}^{2\theta_2} I_{mix}\Big|_w d(2\theta) - \int_{2\theta_1}^{2\theta_2} I_{PS}d(2\theta) \quad (13)$$

where $A_{mix}\big|_w$ and A_{PS} are the integrals of the diffraction intensity in the total range of scattering angle (of interest), from $2\theta_1 \cong 1.5$ to $2\theta_2 \cong 10°$, for the PNC with w
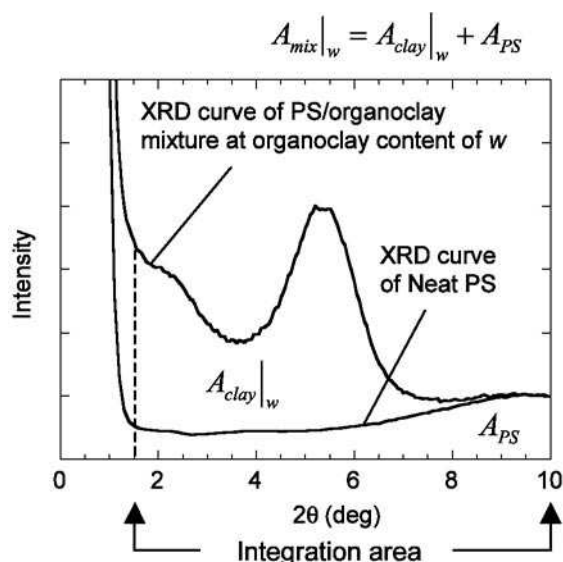
$$A_{mix}\big|_w = A_{clay}\big|_w + A_{PS}$$

Fig. 11. *Definition of A_{PS}, $A_{mix}\big|_w$ and $A_{clay}\big|_w$.*

Fig. 12. *$A_{mix}\big|_w$ as a function of organoclay content for PS based organoclay mixtures.*

wt% of organoclay content and that of neat PS. $I_{mix}\big|_w$ and I_{PS} are the intensities of PNC with w wt% of organoclay and neat PS, respectively. Thus, in the case of not exfoliated PNC, $A_{clay}\big|_w$ should linearly increase with the weight fraction of organoclay in the matrix.

Figure 11 shows the relations between $A_{mix}\big|_w$, A_{PS} and $A_{clay}\big|_w$. Since within the scattering angle of interest A_{PS} is constant, independent of organoclay loading, the following gradient may be defined:

$$S = \frac{\partial A_{clay}\big|_w}{\partial w} = \frac{\partial A_{mix}\big|_w}{\partial w} \qquad (14)$$

If the amount of the X-ray scattering clay does not change with clay loading, the gradient is expected to be constant, i.e., $S = \text{const}$. However, if the extent of exfoliation depends on organoclay content, S will either decrease or increase with w. Thus, when (within interlayer spacing from $\lambda/2\sin\theta_1$ to $\lambda/2\sin\theta_2$) the gradient decreases with organoclay loading, it means that the organoclay progressively exfoliates with the organoclay loading. By contrast, when S increases with organoclay content, the exfoliation is reduced with loading.

Figure 12 shows the $A_{mix}\big|_w$ as a function of organoclay content for the three series of PS-based PNC. The numerical integration of the XRD spectra was carried out from 1.5 to 10°. $A_{mix}\big|_w$ for each PS based organoclay mixtures increases with organoclay content. According to *Eq 12*, in the absence of exfoliation, the dependence should start at the graph origin (0, 0) and increase linearly with w. Drawing such a dependence through the data for dilute systems ($w < 3$ wt%) leads to the conclusion that there is scatterer deficit at higher concentration. While a possibility of increased exfoliation with clay loading cannot be ruled out, this mechanism is unlikely.

There are several possible sources for the XRD peak broadening in a PNC—one being the existence assumed
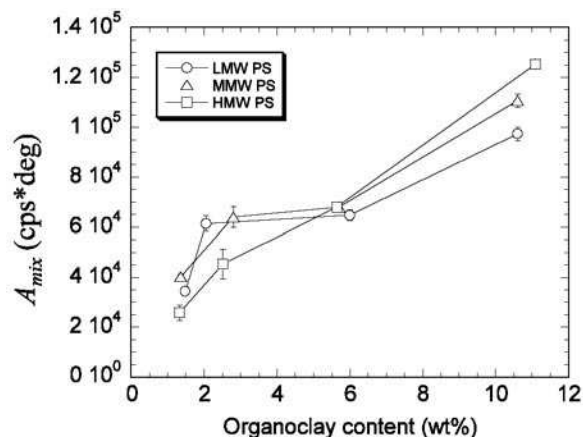
above of a wide variety of clay stacks with a range of d_{001} spacing. Another mechanism of peak broadening is based on the slight imperfections in crystalline lattice of m-layer of clay platelets forming a stack $t = (m - 1) \times d_{001}$ thick. Because of small angle difference between θ_1 and θ_2 between them the destructive interference is incomplete (32). Calculation leads to the following formula credited to Scherrer:

$$t = k\lambda/(B_{1/2}\cos\theta_B); \quad k \cong 0.9 \qquad (15)$$

where λ is the wavelength, $B_{1/2} \cong \theta_1 - \theta_2$ is peak width (in radians) at half peak height ($I_{max}/2$), and $\theta_B \cong (\theta_1 + \theta_2)/2$. From *Eq 15*, the number of clay platelets per average stack with the interlayer spacing d_{001} can be calculated as $m = 1 + t/d_{001}$. Results of these calculations are presented in *Table 6*. Note that in this interpretation, the increased area of the peak is caused by crystalline defects within each individual stack, and not by stacks having different interlayer spacing.

The PVT Behavior

Fitting the coupled *Eqs 7* and *8* to data simultaneously yields the free volume parameter h as a function of pressure and temperature, $h = h(P, T)$, for each composition. Defining the free volume fraction in terms of specific volume, $V = V(P, T)$, and its equivalent at absolute zero, $V_0 = V(P, 0)$; thus $f = 1 - V_0/V$, a correlation between h and f can be found (33), viz. $h \cong 1 - 0.95 V_0/V$. A polynomial expression was recently derived (34):

$$h = a_0 + a_1/\widetilde{V} + a_2\widetilde{T}^{3/2} + a_3/\widetilde{V}^2 + a_4\widetilde{T}^3 \qquad (16)$$

where a_i's are equation parameters (viz. 1.203, -1.929, 10.039, 0.729, -218.42, respectively). Using all five parameters results in standard deviation of data $\sigma = 0.0025$ and the correlation coefficient squared: $r^2 = 0.9997$, but setting $a_3 = a_4 = 0$ gives a reasonable precision ($\sigma = 0.0055$ and $r^2 = 0.998$). Example of the computed $h = h(P, T)$ dependence is presented in *Fig. 13* for neat PS 1301—the relation for other compositions is quite similar. However, in the context of the present paper the interest is to observe how addition of organoclay affects the h-parameter.

**Table 6. Calculated From XRD, the Interlayer Spacing, d_{001} (nm),
and the Number of Platelets per Stack, m, for PNC With Three PS Resins.**

PS	Organoclay (wt%)	d_{001} (nm)		m	
		1st Peak	2nd Peak	1st Peak	2nd Peak
HMW PS	1.3	4.3	1.44		6.5
	2.5		1.54	3.8	5.8
	5.6	4.28	1.61	3.7	4.5
	11.1	4.23	1.65	3.1	4.3
MMW PS	1.4	4.9	1.7	3.3	4.3
	2.8		1.55		4.6
	5.7	4.02	1.75	3.7	4.2
	10.6	4.18	1.65	3.3	4.2
LMW PS	1.5	4.58	1.55	3.1	4.8
	2.1		1.6		4.4
	6.0	4	1.75	3.8	4.4
	10.6	4.2	1.75	3.1	4.4

In *Fig. 14* the relative hole fraction is plotted as a function of organoclay loading, w, at single pressure, $P = 10$ bar, and three temperatures: $T = 360$, 460 and 560 K. The relative quantity is defined as a ratio: h(PNC)/h(PS), thus at any T and P it starts at 1. By contrast, a similar plot for the relative specific volume, V(PNC)/V(PS), vs. w shows a linear decrease in the full range of composition. This behavior is consistent with the constant ratio of densities in the molten state: ρ(organoclay)/ρ(PS) = 1.49.

Recently, in clay-containing PNC of poly-ε-caprolactam (PA-6) the reduction of free volume by 12% to 17% was observed, in the full range of independent variables ($T = 300-590$ K; $P = 1$ to 2000 bar) (35). At the same time, the relative specific volume decreased by ca. 1%. These data were obtained for PNC comprising 2 wt% of MMT pre-intercalated with ω-amino dodecyl acid. Since during the reactive exfoliation the intercalant becomes the end tethering first mer of the matrix PA-6, there was nothing to prevent the macromolecules from becoming

adsorbed on the high-surface-energy clay platelets. The immobilization caused loss of segmental mobility and free volume.

The results reported in this paper are most interesting for two reasons: 1) the degree of intercalation/exfoliation is incomparably lower than that in PA-6/MMT system discussed above, and 2) the organoclay used in the present work contains intercalant forming an intermediate layer between inorganic, high-energy surface of clay platelets and PS matrix. The data presented in *Fig. 14* indicate that in spite of these obstacles, the clay is able to adsorb PS macromolecules, forming an adjacent polymeric layer with low segmental mobility. Furthermore, the data show that the effect is the largest at ca. 4 wt% organoclay, resulting in 4% to 6% loss of the free volume. Using *Eq 5*, the average interaction parameters, energetic: $<\varepsilon^*>$ and volumetric: $<v^*>$, can be
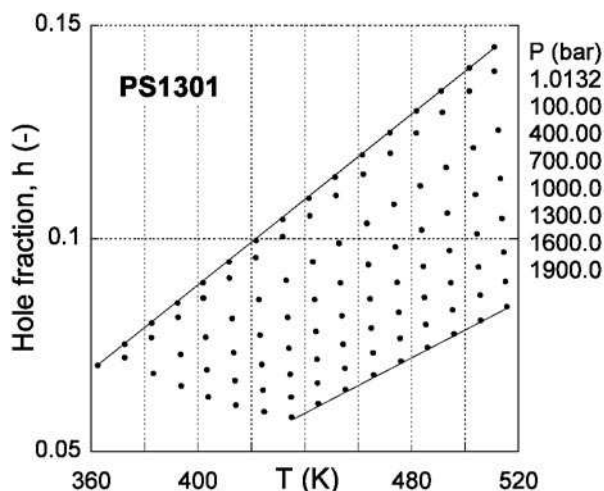

Fig. 13. Hole fraction as a function of temperature for pressures (from the top) P = 1.0132 to 1900 bar for neat PS 1301 (MMW).
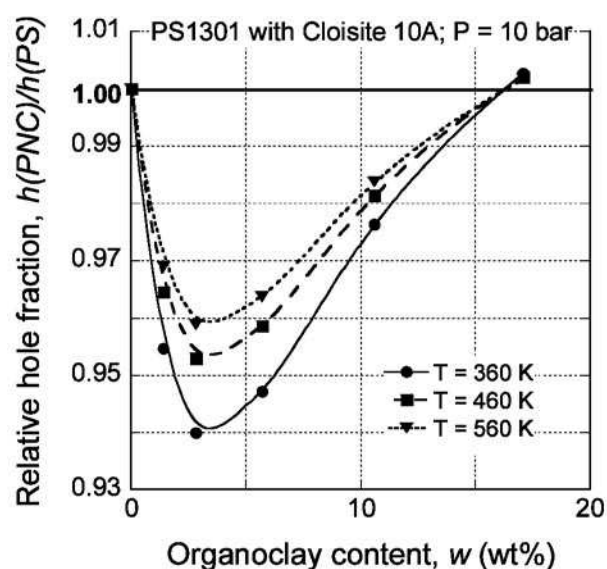

Fig. 14. The relative hole fraction of PS1301 with Cloisite® 10A vs. organoclay concentration, w, at P = 10 bar, and at T = 360, 460 and 560 K.
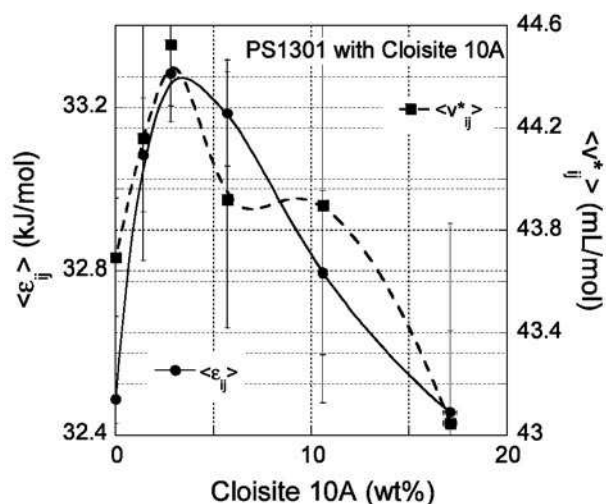
Fig. 15. Average values of the energetic, $<\varepsilon^*>$, and volumetric, $<v^*>$, interaction parameters for PS1301/Cloisite® 10A systems. Data—calculated; lines to guide the eye.

calculated from the reducing parameters, P^*, V^* and T^* (see the last two rows of *Table 5*). The compositional dependence of these parameters is shown in *Fig. 15*.

CONCLUSIONS

Polystyrene-based PNC with commercial organoclay were prepared by melt compounding using a TSE extruder. Three grades of PS with different molecular weight were used. In this paper, we discussed the compounding and characterization of the PNC. The following results were obtained:

1) The residence time and its distribution, as measured by the ultrasonic technique, were independent of the molecular weight of the PS matrix.

2) According to the ultrasonic monitoring, the sound velocity decreases with organoclay content and molecular weight of PS. The attenuation increases with an increase of organoclay content and is almost independent of molecular weight of PS.

3) XRD diffraction results show that there are two peaks on each XRD curve. The 1st peak is located at 2θ of about 2° and is related to intercalation by molten PS macromolecules. The 2nd peak is located at 2θ of about 5.5° and is explained by the reduction of interlayer spacing of organoclay from collapsed swelling agents during the compounding process. The interlayer spacing from the 1st peak increases with organoclay content. In contrast, the spacing corresponding to the 2nd peak decreases with an increase of organoclay content. These findings are independent of molecular weight of PS.

4) TEM analysis indicates that the quality of distributive mixing is reasonably good. However, some large agglomerates persist. Estimation of d_{001}

spacing from the TEM micrographs suggests that the spacing increases as the molecular weight of the polymer decreases. The low-molecular-weight resin appears to produce substantially larger spacing and thus a higher degree of intercalation.

5) The FT-IR results provide evidence for thermal degradation of the onium compound according to the Hofmann reaction, leading to breakdown into benzyl dimethyl amine and a long-chain olefin that undergoes further reaction through oxidation.

REFERENCES

1. M. Alexandre and P. Dubois, *Mater. Sci. Eng. A,* **28**, 1 (2000).
2. L. A. Utracki and M. R. Kamal, *Arabian J. Sci. Eng.,* **27**, 43 (2002).
3. Y. Kojima, A. Usuki, M. Kawasumi, A. Okada, Y. Fukushima, T. Karauchi, and O. Kamigaito, *J. Mater. Res.,* **6**, 1185 (1993).
4. A. Okada, M. Kawasumi, T. Kurauchi, and O. Kamigaito, *Polymer Preprints,* **28(2)**, 447 (1987).
5. A. Okada, M. Kawasumi, A. Usuki, Y. Kojima, T. Kurauchi, and O. Kamigaito, *Mater. Res. Soc. Proc.,* **171**, 45 (1990).
6. A. Okada and A. Usuki, *Mater. Sci. Eng.,* **C3(2)**, 109 (1995).
7. X. Fu and S. Qutubuddin, *Mater. Lett.,* **42**, 12 (2000).
8. C.-R. Tseng, J.-Y. Wu, H.-Y. Lee, and F.-C. Chang, *Polymer,* **42**, 10063 (2001).
9. C.-R. Tseng, J.-Y. Wu, H.-Y. Lee, and F.-C. Chang, *J. Appl. Polym. Sci.,* **85**, 1370 (2002).
10. N. Hasegawa, H. Okamoto, M. Kawasumi, and A. Usuki, *J. Appl. Polym. Sci.,* **74**, 3359 (1999).
11. B. Hoffmann, C. Dietrich, R. Thomann, C. Friedrich, and R. Mülhaupt, *Macromol. Rapid Commun.,* **21**, 57 (2000).
12. C. Park, O. O. Park, J. G. Lim, and H. J. Kim, *Polymer,* **42**, 7465 (2001).
13. J. T. Yoon, W. H. Jo, M. S. Lee, and M. B. Ko, *Polymer,* **42**, 329 (2001).
14. J. Uribe, M. R. Kamal, A. Garcia-Rejon, and L. A. Utracki, *Proceedings of the Polymer Processing Society Annual Meeting,* Guimarães, Portugal (2002).
15. T. D. Fornes, P. J. Yoon, H. Keskkula, and D. R. Paul, *Polymer,* **42**, 9929 (2001).
16. J. Tatibouët and M. A. Huneault, *Intern. Polym. Processing,* **17**, 49 (2002).
17. R. Gendron, J. Tatibouët, J. Guèvremont, M. M. Dumoulin, and L. Piché, *Polym. Eng. Sci.,* **35**, 79 (1995).
18. R. Gendron, L. E. Daigneault, J. Tatibouët, and M. M. Dumoulin, *SPE ANTEC Tech. Papers,* **40**, 167 (1994).
19. M. Marcotte, M. Trigui, J. Tatibouët, and H. S. Ramaswamy, *J. Food Sci.,* **65**, 1180 (2000).

20. D. R. França, C.-K. Jen, K. T. Nguyen, and R. Gendron, *Polym. Eng. Sci.,* **40**, 82 (2000).
21. Z. Sun, C.-K. Jen, and C.-K. Shih, *Proceedings of the Polymer Processing Society Annual Meeting,* Guimarães, Portugal (2002).
22. L. Piché, A. Hamel, R. Gendron, M. M. Dumoulin, and J. Tatibouët, U.S. Patent 5,433,112 (1995).
23. R. Gendron, M. M. Dumoulin, J. Tatibouët, L. Piché, and A. Hamel, *SPE ANTEC Tech. Papers,* **39**, 2256 (1993).
24. R. Simha and T. Somcynsky, *Macromolecules,* **2**, 342 (1969).
25. R. Simha, L. A. Utracki, and A. Garcia-Rejon, *Composite Interfaces,* **8**, 345 (2001).
26. L. A. Utracki, *Polymer Alloys and Blends,* Hanser V., Munich (1989).
27. J. W. Cho, D. R. Paul, H. R. Dennis, and D. L. Hunter, Symposium on *Commercialization of Nanostructured Materials,* Miami, Fla. (2000).
28. J. Zhu, A. B. Morgan, F. J. Lamelas, and C. A. Wilkie, *Chem. Mater.,* **13**, 3774 (2001).
29. D. M. Delozier, R. A. Orwoll, J. F. Cahoon, N. J. Johnston, J. G. Smith, Jr., and J. W. Connell, *Polymer,* **43**, 813 (2002).
30. Sigma-Aldrich Co., *The Aldrich Library of FT-IR Spectra, Edition II,* Vol. 2, Spectrum 2165C (1997).
31. L. J. Bellamy, *The Infra-red Spectra of Complex Molecules, 3rd Ed.,* Chapman and Hall (1975).
32. B. D. Cullity and S. R. Stock, *Elements of X-ray Diffraction, 3rd Ed.,* Chaps. 5 and 12, Prentice-Hall, Upper Saddle River, N.J. (2001).
33. L. A. Utracki and R. Simha, *J. Polym. Sci., Part B: Polym. Phys.,* **39**, 342 (2001).
34. L. A. Utracki and R. Simha, *Macromol. Chem. Phys., Molecul. Theory Simul.,* **10**, 17 (2001).
35. L. A. Utracki, R. Simha, and A. Garcia-Rejon, *Macromolecules,* **36**, 2114 (2003).